Quantum Monte Carlo simulations of driven spin-boson systems

Arnim Lück, Manfred Winterstetter, and Ulrich Weiss
II. Institut für Theoretische Physik, Universität Stuttgart, D-70550 Stuttgart, Germany

C. H. Mak
Department of Chemistry, University of Southern California, Los Angeles, California 90089-0482
(Received 25 March 1998)

A discretized path integral formulation of the real-time dynamics applicable to a general external field is derived for the driven spin-boson model to extend the recently developed real-time Quantum Monte Carlo algorithm to driven systems. Numerical results are obtained for a monochromatic periodic driving force and Ohmic dissipation with a high-frequency cutoff. The impact of an external driving field on the dissipative dynamics is examined for systems with a time-dependent bias as well as a time-dependent interstate coupling matrix element. This method is easily generalized to multistate tight-binding models.
[S1063-651X(98)11411-3]

PACS number(s): 05.30.−d

I. INTRODUCTION

The spin-boson model, a two-state system coupled bilinearly to a harmonic reservoir, is the simplest model of quantum tunneling in a potential interacting with a dissipative environment. If the tunneling motion can be described by a double-well potential with a localized state in each well and if these states are well separated from other high-lying states, the dynamics of the quantum particle can be confined to a two-dimensional Hilbert space. The dynamics is then fully described by the time evolution of the *reduced density matrix* of the two-state system. The spin-boson model has found widespread applications to various biological, chemical, and physical systems. For example, it has been used to model the tunneling of atoms between the tip of an atomic-force microscope and a surface [1,2], for studying the dynamics of the magnetic flux in a superconducting interference device [3], and for electron transfer reactions [4–7]. A multistate generalization of the spin-boson system has also been used to study the dynamics of the ultrafast charge separation in bacterial photosynthesis [8–10]. (For other applications, see [11] and references therein.)

Within the path integral formulation of quantum mechanics [11–14], it is a straightforward procedure to eliminate the reservoir if its dynamics may be regarded as linear. The effect of the environment is then captured by an influence functional giving rise to time-nonlocal correlations between different segments of the path [15,13,11]. In this approach, any number of environmental modes, even an infinity of them, can be treated conveniently by tracing out the bath analytically. However, the time-nonlocal interactions in the influence functional make the evaluation of the path integral difficult. If the coupling to the environmental modes is weak and/or the temperature is high, the Markov approximation can be applied, which makes the interactions local and this brings about substantial simplifications. However, many of the interesting properties of the spin-boson model occur at low temperatures where the Markovian approximation is invalid. Although substantial progress has been made on the analytical side [16–20], numerical calculations are imperative for low temperatures and intermediate coupling since no cutoff in the range of the interaction can be assumed in this parameter regime. During the past several years, numerical methods have been developed to carry out dynamical simulations [7,9,21–25] for the spin-boson system in various parameter regions. All these simulations, to various degrees, suffer from the ubiquitous *dynamical sign problem* in the intermediate and long time regimes. (For reviews see [26–28].)

Stimulated by the discovery that tunneling in the bare two-state system can be completely suppressed by a monochromatic driving field with suitably chosen amplitude and frequency [29–31], driving-induced suppression of tunneling in dissipative systems has attracted considerable interest. Even in the presence of dissipation, one finds that the effect persists [32–37]. The significance of this finding for electron transfer reactions in a polar solvent was discussed in Refs. [38,39]. More recently, quantum Monte Carlo simulations demonstrating the equivalence of a nonequilibrium initial preparation on the dynamics of an electron transfer system to that of a driven spin-boson system were presented in [40]. Also interesting is the suggestion that external driving may be able to invert the populations of donor and acceptor states [34,39,41]. Chemically, this has important implications because it may enable the activation of certain chemical reactions by external driving fields. In addition to these studies, several interesting contributions to the field of driven dissipative systems have also been published in recent years (see, for example, Refs. [42–48]). For a comprehensive review on driven quantum tunneling (in undamped as well as damped systems) see [49]. Most of the previous work on driven systems deals only with driving fields that couple to diagonal operators of the system. Little attention has been given to off-diagonal driving so far [37].

Analytically, the questions surrounding driven tunneling systems are numerous and complex. In contrast to the undamped driven system, except for theories with uncontrolled approximations, a rigorous analytical treatment of the dissipative case has not been found. Hence it is crucial that a nonperturbative approach be developed for treating this

problem in the presence of a general time-dependent driving field in order to examine regions of the parameter space that are inaccessible to any approximate methods.

Real-time quantum Monte Carlo (QMC) simulations enable us to study the short time dynamics of driven systems in a numerically exact manner. Approximate methods that may be useful for longer propagation times can then be tested by comparison. With these, we are able to reliably determine the range of validity of the various approximations applied to driven dissipative systems. There are also numerous systems that exhibit a fast enough relaxation for the QMC simulations to be able to cover the entire time interval of interest.

Another area where the techniques presented in this paper are pertinent is in the simulations of pump-probe experiments of large molecules. During the past decade, there has been substantial progress in the experimental study of ultrafast intramolecular processes using ultrashort laser pulses to excite and probe electronic populations. Therefore, it is necessary to take into account the effect of the time dependence of the excitation field as well as the measurement pulse in numerical simulations (see [50] for a review and references).

The paper is organized as follows. In Sec. II the discretized path integral representation for the driven spin-boson system is introduced and emphasis is put on the modifications due to external driving. In Sec. III we apply the path integral representation to derive the QMC algorithm. Section IV discusses the numerical results. In Sec. V some conclusions are drawn and an outlook on possible future work is given.

II. TROTTER PATH INTEGRAL FOR THE DRIVEN SPIN-BOSON MODEL

We study a two-state system that is driven by a time-dependent force and at the same time coupled to a dissipative bosonic bath. In contrast with most of the work reported on the driven spin-boson system to date, the discretized path integral (PI) representation given in this section assumes a general form for the driving force, which can couple either to diagonal operators of the two-state system or to the intersite coupling matrix elements or both.

The Hamiltonian of the driven spin-boson system is given by

$$H = H_0(t) + H_b + H_{\rm int}. \tag{1}$$

$H_0(t)$ is the Hamiltonian of the bare two-state system

$$H_0(t) = \frac{\epsilon(t)}{2}\sigma_z - \frac{\Delta(t)}{2}\sigma_x, \tag{2}$$

with general time-dependent driving fields $\epsilon(t)$ and $\Delta(t)$, where σ_z and σ_x are Pauli matrices. A field coupled to σ_z gives us a time-dependent bias, while a force coupled to σ_x describes a time-dependent intersite coupling. The Hamiltonian of the harmonic bath is given by

$$H_b = \sum_\alpha \left(\frac{p_\alpha^2}{2m_\alpha} + \frac{m_\alpha \omega_\alpha^2}{2} x_\alpha^2 \right) I, \tag{3}$$

where I is the identity in the Hilbert space of the two-state system and the interaction of the two-state system with the bath is given by

$$H_{\rm int} = \frac{1}{2}\sum_\alpha \left(-c_\alpha x_\alpha q_0 \sigma_z + \frac{c_\alpha^2 q_0^2}{4 m_\alpha \omega_\alpha^2}\sigma_z^2 \right), \tag{4}$$

where the two tight-binding states are at positions $\pm q_0/2$. We set $q_0^2 = 1$ in the remainder of this paper.

The influence of the bosonic bath on the two-state system is captured by the spectral density

$$J(\omega) = \frac{\pi}{2}\sum_\alpha \frac{c_\alpha^2}{m_\alpha \omega_\alpha}\delta(\omega - \omega_\alpha). \tag{5}$$

In the numerical calculations presented in this work we assume a continuous spectral density of Ohmic form

$$J(\omega) = 2\pi\alpha\omega q_0^2 \exp\left(-\frac{\omega}{\omega_c}\right). \tag{6}$$

In our notation α is the dimensionless Kondo parameter that describes the strength of the linear system-bath coupling and ω_c is a high-frequency cutoff setting the typical time scale of the dynamics of the bath. Our approach, however, is not restricted to a certain form of the spectral density. In principle, any number of discrete modes as well as any continuous spectral density can be treated. The systems described by the Hamiltonian (1) exhibit a deterministic force represented by the implicitly time-dependent two-state system Hamiltonian as well as a stochastic force originating from the coupling to the harmonic reservoir.

We calculate the expectation value $\langle \sigma_z \rangle_t$ of the system out of an initially prepared state $|\varphi_i>$, with the bath in thermal equilibrium by itself under what is commonly called factorized initial conditions ($\hbar$ is set to unity throughout this paper)

$$\langle \sigma_z \rangle_t = \langle \varphi_i | \left\langle \left[T^\dagger \exp\left(i\int_0^t dt' H(t') \right) \right] \times \hat{\sigma}_z \left[T \exp\left(-i\int_0^t dt' H(t') \right) \right] \right\rangle_\beta |\varphi_i\rangle. \tag{7}$$

Here $\langle\ \rangle_\beta$ denotes the thermal average over the bath. T and $T^\dagger$ are the time-ordering operator and anti-time-ordering operator of the exponential. In our notation, $|\varphi_s\rangle$ denotes the tight-binding state that corresponds to the site s. In principle, the methods developed here can also be extended to nonfactorizing initial states.

In order to evaluate $\langle \sigma_z \rangle_t$ in Eq. (7) numerically we construct a discretized PI expression. In the first step, the propagation time t is divided into N time slices of equal length $\varepsilon = t/N$ and at each of the discretization points a complete basis of the two-state system is inserted. The exact short time propagator for the jth interval $U_j = T\exp[-i\int_{(j-1)\varepsilon}^{j\varepsilon} d\tau H(\tau)]$ is replaced by the symmetric second-order propagator

$$U_j^{\rm sym} = e^{-i\varepsilon(H_b+H_{\rm int})/2} \times \left[T\exp\left(-i\int_{(j-1)\varepsilon}^{j\varepsilon} d\tau H_s(\tau)\right)\right] e^{-i\varepsilon(H_b+H_{\rm int})/2} = e^{-i\varepsilon(H_b+H_{\rm int})/2}\tilde{U}_j^{\rm free} e^{-i\varepsilon(H_b+H_{\rm int})/2}, \quad (8)$$

which factorizes in the system and bath degrees of freedom. The propagator of the driven two-state system alone is now calculated numerically by introducing a subgrid of length ε' within each elementary time interval with $M\varepsilon' = \varepsilon$. Within each subinterval the functions $\varepsilon(t)$ and $\Delta(t)$ are approximated by constants ε_{jk} and δ_{jk}, respectively. The propagators for the subintervals $U_{jk}^{\rm free}$ can then be evaluated analytically, giving

$$\tilde{U}_j^{\rm free} \approx \prod_{k=1}^{M} U_{jk}^{\rm free}. \quad (9)$$

Being a product of unitary propagators for each subinterval, the free propagators $\tilde{U}_j^{\rm free}$ on the coarser grid are unitary, independent of the number of subintervals M. Notice that the decomposition of the full Hamiltonian into a part that acts on the Hilbert space of the two-state system and a part acting on the bath degrees of freedom is not unique. The contribution stemming from $\epsilon(t)\sigma_z$ in Eq. (2) can be included in H_{int} or in H_s. Thus the bias of the system can be interpreted either as a part of the interaction Hamiltonian or as a part of the free two-state system.

Using the second-order approximations $U_j^{\rm sym}$ for the exact propagators we obtain

$$\langle\sigma_z\rangle_t \approx \langle\varphi_i| \left\langle \left[\prod_{j=1}^{N} U_j^{\rm sym}\right]^{\dagger} \hat{\sigma}_z \left[\prod_{j=1}^{N} U_j^{\rm sym}\right] \right\rangle_{\beta} |\varphi_i\rangle. \quad (10)$$

For a fixed propagation time $T=\varepsilon N$ the limit $N\to\infty$ gives the exact expression for $\langle\sigma_z\rangle_t$ according to the Trotter theorem [51]. Inserting the identity in the Hilbert space of the two-state system at each intermediary time yields a discretized double path sum for the expectation value (10). It may be written in the form

$$\langle\sigma_z\rangle_t \approx \sum_{b_{N-1},\ldots,b_1} \sum_{f_{N-1},\ldots,f_1} \times \langle\varphi_i|\langle U_1^{\rm sym\dagger}\hat{P}_{b_1} U_2^{\rm sym\dagger}\hat{P}_{b_2}\cdots U_N^{\rm sym\dagger}\hat{\sigma}_z \times U_N^{\rm sym}\hat{P}_{f_{N-1}} U_{N-1}^{\rm sym}\hat{P}_{f_{N-2}}\cdots U_2^{\rm sym}\hat{P}_{f_1} U_1^{\rm sym}\rangle_{\beta}|\varphi_i\rangle. \quad (11)$$

Here, the forward and backward paths are specified by vectors of dimension $N+1$, $\mathbf{f}^t=(f_0,f_1,\ldots,f_N)^t$, and $\mathbf{b}^t=(b_0,b_1,\ldots,b_N)^t$, in which the first components are specified by the initial state $|\varphi_i\rangle$. The operators $\hat{P}_{\pm}$ are the projectors on the two-state system states $|\varphi_{\pm}\rangle$, respectively. The possible numerical values assigned to the residual N components of these vectors are ± 1 according to the particular state of the two-state system onto which the system is projected at the corresponding intermediate time. As the elementary propagators given by Eq. (8) factorize in the system and bath degrees of freedom, the contribution of each double path in Eq. (11) also factorizes. The piecewise constant function corresponding to the forward path labeled by the vector $\mathbf{f}^t$ is given by

$$f(t)=f_0 \quad \text{for} \quad t\epsilon[0,\tfrac{1}{2}\varepsilon],$$
$$f(t)=f_j \quad \text{for} \quad t\epsilon[(j-\tfrac{1}{2})\varepsilon,(j+\tfrac{1}{2})\varepsilon],$$
$$f(t)=f_N \quad \text{for} \quad t\epsilon[(N-\tfrac{1}{2})\varepsilon,N\varepsilon].$$

The function $b(t)$ corresponding to the backward path is defined analogously. Performing the trace over the bath degrees of freedom results in the Feynman-Vernon influence functional [11,15] whose ensuing form suggests switching from the forward and backward paths to the symmetric $\boldsymbol{\eta}$ and antisymmetric combinations $\boldsymbol{\chi}$, which describe propagation along the diagonal and excursions away from the diagonal of the density matrix, respectively. The former is the quasiclassical path, while the latter describes quantum fluctuations. The piece-wise constant funcions $\eta(t)$ and $\chi(t)$ are given by

$$\eta(t)=f(t)+b(t)+2\overline{q}, \quad (12)$$

$$\chi(t)=f(t)-b(t). \quad (13)$$

The evolution of the expectation value is then described by the discretized path sum

$$\langle\sigma_z\rangle_t = \sum_{\{\boldsymbol{\chi},\boldsymbol{\eta}\}} P_{\rm free}(\boldsymbol{\chi},\boldsymbol{\eta})\exp[-\Phi(\boldsymbol{\chi},\boldsymbol{\eta})]. \quad (14)$$

Here $P_{\rm free}(\boldsymbol{\chi},\boldsymbol{\eta})$ represents the contribution from the double path $(\boldsymbol{\chi},\boldsymbol{\eta})$ for free propagation of the two-state system and $\exp[-\Phi(\boldsymbol{\chi},\boldsymbol{\eta})]$ describes the influence of the environment [11]. Further, $\Sigma_{\{\chi_j,\eta_j\}}$ denotes the summation over all possible arrangements of paths for fixed boundary values. Since the system starts out at time zero from a diagonal state of the reduced density matrix and arrives at time t again in a diagonal state, the respective $\boldsymbol{\chi}$ components are zero.

The influence functional $\Phi[\boldsymbol{\chi},\boldsymbol{\eta}]$ is given by

$$\Phi[\boldsymbol{\chi},\boldsymbol{\eta}] = \int_0^t dt_2 \int_0^{t_2} dt_1 \chi(t_2)\chi(t_1)L'(t_2-t_1) - i\int_0^t dt_2\int_0^{t_2} dt_1 \chi(t_2)\,\eta(t_1)L''(t_2-t_1) + \frac{i\mu}{2}\int_0^t dt_1 \chi(t_1)\,\eta(t_1), \quad (15)$$

where $L(t)=L'(t)+iL''(t)$ is the bath correlation function [11,7] and

$$\mu = \sum_{\alpha} \frac{c_\alpha^2}{m_\alpha\omega_\alpha^2} = \frac{2}{\pi}\int_0^{\infty} d\omega \frac{J(\omega)}{\omega} \quad (16)$$

is a measure of the coupling strength to the bath degrees of freedom. In the Ohmic case, we have $\mu=\alpha\omega_c$. The bath correlation function is defined by [11,8]

$$L(t)=\frac{1}{\pi}\int_0^\infty d\omega\, J(\omega)\ \ [\coth(\beta\omega/2)\cos\omega t - i\sin\omega t], \tag{17}$$

where $\beta=1/k_BT$ is the inverse temperature.

According to the construction of the discretized path integral, the functions $\chi(t)$ and $\eta(t)$ are piecewise constant. Upon performing the integrations over the elementary intervals, the influence functional $\Phi[\boldsymbol{\chi},\boldsymbol{\eta}]$ may be written in the form

$$\Phi[\boldsymbol{\chi},\boldsymbol{\eta}]=\sum_{j=1}^{N-1}\sum_{k=0}^{j}(\chi_jL'_{jk}\chi_k - i\chi_jL''_{jk}\eta_k), \tag{18}$$

where L'_{jk} and L''_{jk} are the real and imaginary part of the expressions

$$\begin{aligned} L_{jk}&=\int_{(j-1/2)\varepsilon}^{(j+1/2)\varepsilon}dt_2\int_{(k-1/2)\varepsilon}^{(k+1/2)\varepsilon}dt_1L(t_2-t_1)\\ &\quad \text{for}\quad N>j>k\geqslant 1,\\ L_{jj}&=\int_{(j-1/2)\varepsilon}^{(j+1/2)\varepsilon}dt_2\int_{(j-1/2)\varepsilon}^{t_2}dt_1L(t_2-t_1)+i\frac{\mu}{2}\varepsilon\\ &\quad \text{for}\quad N>j>1,\\ L_{j0}&=\int_{(j-1/2)\varepsilon}^{(j+1/2)\varepsilon}dt_2\int_0^{\varepsilon/2}dt_1L(t_2-t_1)\quad \text{for}\quad j\geqslant 1. \end{aligned} \tag{19}$$

For the Ohmic form (6) of the spectral density, the matrix elements L_{jk} can be evaluated in analytic form [8].

The construction of the discretized PI given above for the driven spin-boson system based on the propagator (8) is applicable to a general driving force. If the two-state system is driven diagonally, the impact of the driving force can be included in the influence functional. The propagator of the bare two-state system is then time independent and the changes in the corresponding algorithm are minor. In addition to the influence functional encapsulating the influence of the stochastic force (18), a contribution representing the deterministic force

$$\Phi_{\rm det}[\boldsymbol{\chi}]=i\int_0^{N\varepsilon}d\tau\,\chi(\tau)\varepsilon(\tau) \tag{20}$$

must be added to the influence functional.

The discretized path sum (14) with Eq. (18) is a convenient starting point for performing real-time QMC simulations of dissipative tight-binding models [7,8]. Note that all the influence from the solvent is contained in the matrix elements L_{jk}. It is also important that the influence functional is bilinear in the off-diagonal variable χ, while it depends only linearly on the quasiclassical coordinate η. We would like to point out that the construction of a discretized PI given here can also serve as a starting point for alternative numerical methods such as the tensor multiplication scheme [23] or the path class summation [24]. The generalization of this procedure to tight-binding systems with several degrees of freedom is also straightforward.

III. QMC ALGORITHM

In this section we briefly review the QMC algorithm (see [26]) with emphasis on the modifications that are necessary to account for a generalized driving field. The time evolution of the bare two-state system can be calculated numerically exactly by repeated applications of the free propagators $\tilde{U}_j^{\rm free}$. In the Markovian limit, the dynamics of the density matrix of the two-state system can then be generated by repeated matrix multiplications of the elementary propagators of the density matrix of the two-state system

$$V_j=[(\tilde{U}_j^{\rm free})^\dagger\tilde{U}_j^{\rm free}](\chi_j,\eta_j;\chi_{j-1},\eta_{j-1}). \tag{21}$$

Unfortunately, this procedure does not work in the non-Markovian case.

In the general non-Markovian case, we need to address the nonlocalness of the influence functional. Now suppose that the paths under consideration consist of N elementary time slices and that the quantum fluctuations given by the vector $\boldsymbol{\chi}$ are fixed. At each interval where the quantum fluctuation is zero (corresponding to the diagonal of the density matrix of the two-state system) the quasiclassical variable can take the values ±1 and vice versa. Thus, to a given $\boldsymbol{\chi}$ configuration there corresponds a manifold of $\boldsymbol{\eta}$ configurations. We now show that for a fixed $\boldsymbol{\chi}$ configuration the sum over the remaining quasiclassical degrees of freedom can be performed by matrix multiplication. As can be seen from Eq. (18), the real part of the influence functional depends on the quantum fluctuations only (and is thus the same for all paths for a given $\boldsymbol{\chi}$ configuration). For a given $\boldsymbol{\chi}$ sequence Eq. (21) reduces to a set of 3×3 matrices in the η variable denoted $V_j[\boldsymbol{\chi}]$. Because the imaginary part of the influence functional depends only linearly on both the quantum fluctuations and the quasiclassical degrees of freedom, the elementary propagators of the density matrix of the bare two-state system can be modified to take into account the contribution stemming from the imaginary part of the influence functional depending on the actual time interval

$$\tilde{x}_j=\exp\left(i\eta_j\sum_{l=j+1}^{N}\chi_lL''_{lj}\right). \tag{22}$$

The resulting modified elementary propagators of the reduced density matrix

$$\tilde{V}_j[\boldsymbol{\chi}]=\tilde{x}_jV_j[\boldsymbol{\chi}] \tag{23}$$

take into account all interactions of the actual interval j with all later intervals with $l>j$. Consequently, the summation over all quasiclassical degrees of freedom corresponding to $\boldsymbol{\chi}$ can be written as

$$\langle\sigma_z\rangle_t[\boldsymbol{\chi}]=\exp(-\mathrm{Re}\,\Phi[\boldsymbol{\chi}])\prod_{j=1}^{N}\tilde{V}_j[\boldsymbol{\chi}], \tag{24}$$

where at the initial time $t=0$ we have $\eta_0=1$ and $\chi_0=0$, whereas at the final time $t=N\varepsilon$ the boundary values are $\eta_N=\pm1$ and $\chi_N=0$, reflecting the fact that all double paths that contribute to $\langle\sigma_z\rangle_t$ start and end in the diagonal of the reduced density matrix. Thus the summation over the quasi-

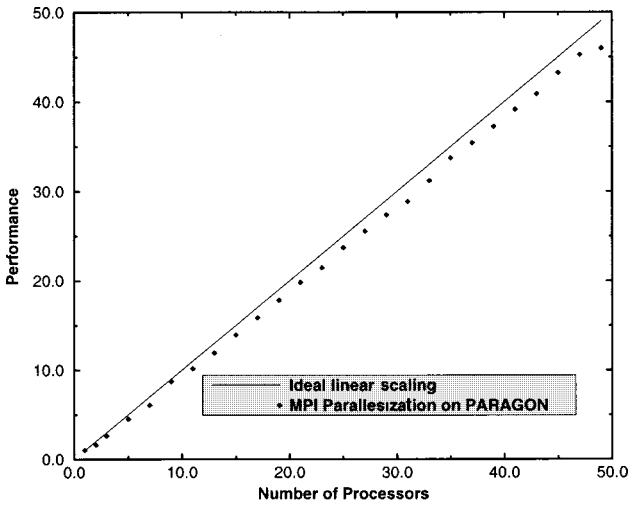

FIG. 1. Typical scaling of a quantum Monte Carlo simulation on a Paragon parallel computer. Each point is an average of 10 MC runs with 500 000 sample paths and 40 time slices for the same physical model. The MC runs are started separately on different processors to eliminate the influence of message passing between specific sets of processors of the Paragon architecture using a message passing interface (MPI).

classical degrees of freedom is performed in a numerically stable and effective manner by matrix multiplication reducing the ubiquitous sign problem of real-time QMC simulations remarkably. The expectation value $\langle \sigma_z \rangle_t$ is now given by the remaining summation over the quantum fluctuations $\boldsymbol{\chi}$,

$$\langle \sigma_z \rangle_t = \sum_{\boldsymbol{\chi}} \langle \sigma_z \rangle_t [\boldsymbol{\chi}]. \tag{25}$$

Because $Q'(t)$ in Eq. (15) is symmetric for any spectral density function $J(\omega)$, the real part of the influence functional can be written in a symmetrized way $\mathrm{Re}\,\Phi[\boldsymbol{\chi}] = \frac{1}{2}\Sigma_{j,k=1}^{N-1} \chi_j L'_{jk} \chi_k$. Thus the first factor in Eq. (24) defines a Gaussian measure in the space of the $\boldsymbol{\chi}$ configurations. The Monte Carlo sampling is therefore reduced to the stochastic integration of the quantities $\langle \sigma_z \rangle_t [\boldsymbol{\chi}]$. For a detailed description of the real-time Quantum Monte Carlo algorithm we refer the reader to [26]. The essential modification of the algorithm in comparison with the undriven case consists of replacing the time-independent free propagator by the time-dependent free propagators $\tilde{U}_j^{\mathrm{free}}$.

Finally, let us focus on the technical features of the QMC simulation. A central problem of the QMC method is the control of the statistical error. It is proportional to $1/\sqrt{N_s}$, where N_s is the number of accepted samples. These samples are statistically independent and can therefore be calculated simultaneously on different CPUs. This makes the QMC simulations a perfect candidate for massive parallelization on distributed memory architectures. As is illustrated in Fig. 1, the performance (defined as the longest CPU time that occurred during the simulation, scaled by the monoprocessor time of the simulation: $P(n) = T_{\max,1}/T_{\max,n}$, where $T_{\max,n}$ is the longest CPU-time that occurred calculating 500 000 samples on n processors) scales almost linearly with the number of processors. With the availability of high-performance computers with distributed memory architecture (e.g., the Cray T3E computer) the applicability of the method will be enhanced drastically.

TABLE I. Model parameters.

Model	α	ω_c	β	ϵ_0
Ia	0.25	$5\Delta_0$	$2/\Delta_0$	$2\Delta_0$
Ib	0.25	$5\Delta_0$	$2/\Delta_0$	$-2\Delta_0$
II	0.5	$5\Delta_0$	$10/\Delta_0$	$-0.75\Delta_0$
III	0.25	$10\Delta_0$	$10/\Delta_0$	0

IV. RESULTS AND DISCUSSION

In this section we present results of the simulations that are aimed at studying the impact of an external periodic driving force on the dynamics of the dissipative two-state system. If an undriven system is exposed to a biasing force it may be essentially trapped in the initial localized state or it may tunnel through the barrier depending on the sign of the bias, with the asymptotic values of $\sigma_z(t)$ being very close to ± 1 on a time scale of several periods of the interstate coupling frequency. Now the question arises whether one can either induce a transition to the energetically higher-lying state or suppress the incoherent tunneling by an external field [44,47]. The study of both of these processes is essential for understanding the design of molecular switches.

While in most of the literature on the driven spin-boson model a driving force coupling diagonally to the two-state system is studied, *we treat both diagonal and off-diagonal coupling* to the external force. In this work we restrict our attention to monochromatic driving of the form

$$\epsilon(t) = \epsilon_0 + \epsilon_a \sin(\nu_\epsilon t) \tag{26}$$

and

$$\Delta(t) = \Delta_0 + \Delta_a \sin(\nu_\Delta t). \tag{27}$$

All frequencies are given in units of the intersite coupling matrix element Δ_0.

To gain a global perspective on the qualitative dynamical behaviors of the driven spin-boson model in parameter regions where analytical approximations are likely to fail, we have chosen to study in particular three different models, which we denote by I, II, and III. The parameters for each model are given in Table I. A relatively weak system-bath coupling strength, low temperatures, and a moderate cutoff frequency define a parameter regime that is hardly accessible to analytical methods and therefore a regime that can only be addressed by real-time QMC simulations. Though QMC simulations are computationally expensive, they are the only viable method here.

A. Diagonal driving force

In this section we discuss results for various models subject to a diagonal driving force. Results for nondiagonal driving are presented in Sec. IV B.

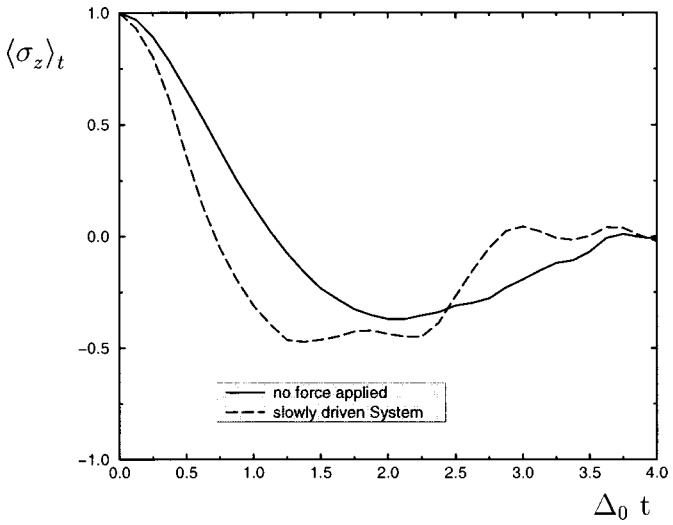

FIG. 2. $\langle\sigma_z\rangle_t$ for model Ia for different monochromatic driving coupled diagonally. The solid curve corresponds to the undriven case. The dashed line has frequency $\nu_\epsilon=\Delta_0/2$ and amplitude $\epsilon_a=\Delta_0/2$ and the dotted curve frequency $\nu_\epsilon=2\Delta_0$ and amplitude $\epsilon_a=10\Delta_0$.

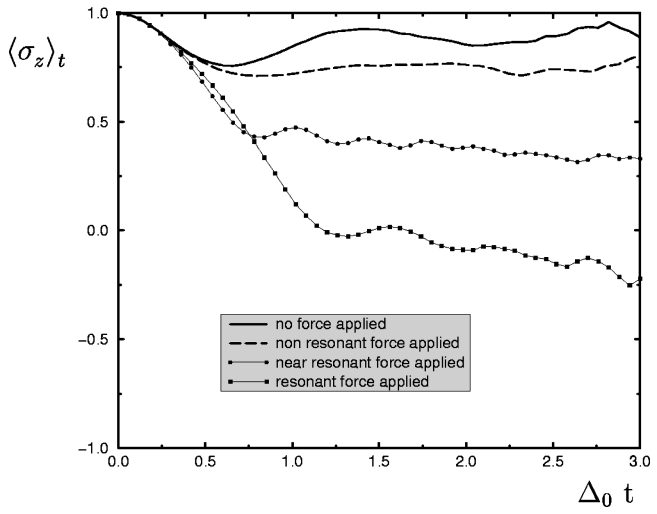

FIG. 3. $\langle\sigma_z\rangle_t$ for model Ib for different monochromatic driving coupled diagonally. The solid curve corresponds to the undriven case. The dashed line has frequency $\nu_\epsilon=\Delta_0$ and amplitude $\epsilon_a=\Delta_0/2$ and the dotted curve frequency $\nu_\epsilon=0.4\Delta_0$ and amplitude $\epsilon_a=6\Delta_0$. The squares correspond to a frequency $\nu_\epsilon=0.3\Delta_0$ and an amplitude $\epsilon_a=4\Delta_0$.

1. Model I

Model I has a moderate dissipation $\alpha=0.25$, with a relatively large cutoff frequency $\omega_c=5\Delta_0$ typical of electron transfer systems and a moderate temperature $\beta=2/\Delta_0$. We have investigated the effects of external driving on both the cases of a forward (model Ia) and a backward (model Ib) bias. Figure 2 shows the expectation value of the population difference $\langle\sigma_z\rangle_t$ for forward bias ($\epsilon_0=2\Delta_0$), model Ia. Numerical results for the undriven system are also shown as the solid line in the same figure for comparison.

The results for the undriven system indicate that the system exhibits a fast transfer to the lower-lying localized state with some low-amplitude coherent oscillations. This fast transfer is expected due to the relatively large forward bias applied to the system. However, the application of an external driving field can substantially alter the qualitative behavior of the dynamics. If a weak driving force with $\epsilon_a=\Delta_0/2$ and $\nu_\epsilon=\Delta_0/2$ is applied, the tunneling rate is reduced only moderately (dashed line in Fig. 2) compared to the undriven system. However, if the driving amplitude is increased to $\epsilon_a=10\Delta_0$ and the frequency to $\nu=2\Delta_0$, the system is essentially trapped in the initial state on the timescale depicted in Fig. 2 (dotted line). This result confirms the general expectation that a high-frequency driving field is able to localize a tunneling system in the donor state, even in the presence of a strong forward bias, which in the undriven case would have greatly enhanced the tunneling transfer to the acceptor.

In Fig. 3 the dynamics for the same system but with a backward bias $\epsilon_0=-2\Delta_0$, model Ib, is shown for different periodic external forces. Again the solid line corresponds to the undriven system. In this case, since the system is biased negatively and heavily, the undriven system is essentially trapped in the initial state (solid line). There are coherent oscillations that die out almost completely on the time scale shown in this figure. For this case, the application of an external driving field can also markedly change the dynamical behavior. Whereas in model Ia with the forward bias the driving field can suppress tunneling transfer, here for Model Ib with the backward bias, the driving field can actually *enhance* the tunneling transfer. When an external field with amplitude $\epsilon_a=\Delta_0/2$ and a relatively high frequency $\nu=\Delta_0$ is applied, after a short time the transfer is almost completely turned off with only a low-amplitude oscillation of the period of the driving force. However, if the frequency of the driving force is reduced to $\nu_\epsilon=0.3\Delta_0$ and the amplitude is raised to $\epsilon_a=4\Delta_0$, the terminal population of the initial state is now reduced to about 0.40 (squares), indicating that the driving field is able to induce tunneling transfer from the donor to the acceptor state at a much higher efficiency. These conditions chosen for the driving field represent the optimal choice for maximizing the transfer efficiency for the tight-binding particle to undergo a transition out of the energetically lower-lying state due to external driving. This result illustrates the remarkable possibility of using an external field to activate a tunneling transition that would have been impossible without the driving field. If the amplitude is further increased beyond the opitmal value, the tunneling rate decreases again, as can be seen from the dotted curve, which corresponds to a driving amplitude of $\epsilon_a=6\Delta_0$.

It should be noted that the frequencies of the external force for the results depicted by the dotted line and the squares in Fig. 3 are much lower than the intersite coupling element. Thus the driving can be considered adiabatic on the time scale of the plot. A higher-frequency driving field, when applied to model Ia, would not further affect the dynamics of the trapped system, except by inducing low-amplitude oscillations on the otherwise static population. Therefore, plots for higher driving frequencies have been omitted. Incidentally, the small-amplitude oscillations seen in Fig. 3 at intermediate times for the backward biased system are not related to the frequency of the driving force, but instead to its *amplitude.* These oscillations are expected to vanish with time

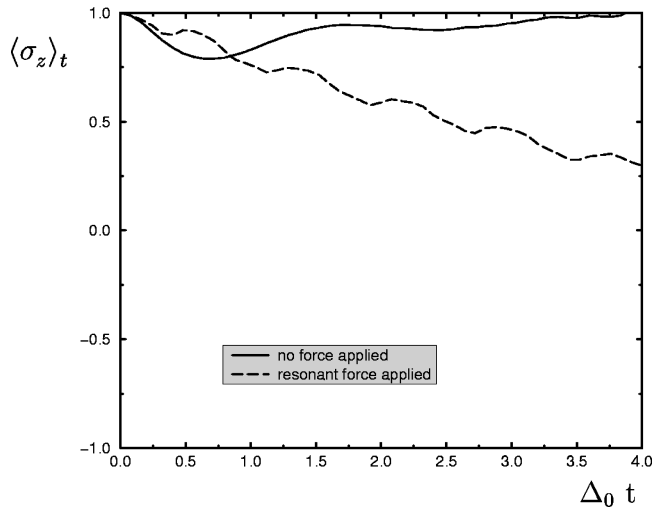

FIG. 4. $\langle\sigma_z\rangle_t$ for model II for different monochromatic driving coupled diagonally. The solid curve corresponds to the undriven case. The dashed line has frequency $\nu_\epsilon=4\Delta_0$ and amplitude $\epsilon_a=10\Delta_0$.

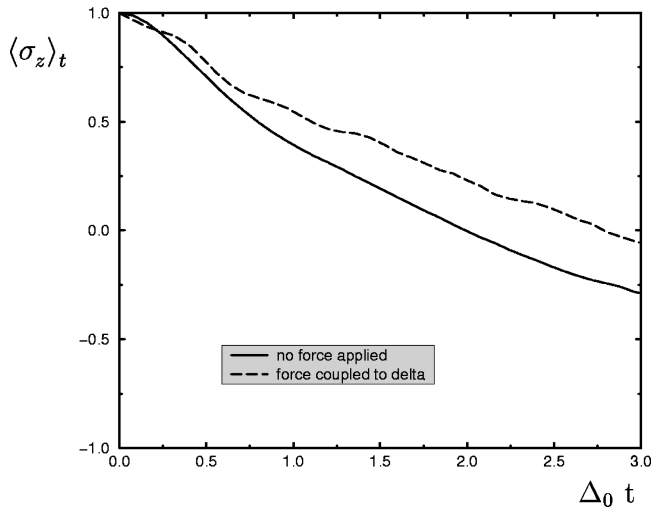

FIG. 5. $\langle\sigma_z\rangle_t$ for model Ia for different monochromatic driving coupled off diagonally. The solid curve corresponds to the undriven case. The dashed line has frequency $\nu_\Delta=\Delta_0$ and amplitude $\Delta_a=0.9\Delta_0$.

since the dynamics must exhibit the frequency of the driving force in the asymptotic limit.

2. Model II

We now turn to model II. Compared to model I, this system is characterized by a stronger dissipation ($\alpha=0.5$) but a weaker backward bias ($\epsilon=-0.75\Delta_0$) and at a low temperature ($\beta=10/\Delta_0$). The solid line in Fig. 4 again depicts $\langle\sigma_z\rangle_t$ without periodic driving. Again due to the backward bias, the undriven system is essentially trapped in the initial state. The dashed line shows the dynamics for a diagonal driving with a periodic force ($\epsilon_a=10\Delta_0$ and $\nu_\epsilon=4\Delta_0$). Despite the stronger damping here compared to model Ib, the system still exhibits a transition toward the higher-lying localized state even on the relatively short time scale of the plot. In contrast with the plateaulike dynamics of model Ib shown in Fig. 3, $\langle\sigma_z\rangle_t$ of model II is basically linear with a characteristic oscillatory structure superposed on top of it. Within the time regime covered by the QMC simulations we do not observe a plateau in the population for model II.

In this case, the oscillations of the driven system actually reflects the periodicity of the driving force. Since the coupling is strong, contributions stemming from higher harmonics show up in the transient population. In contrast, these harmonics are not present in the results for model Ib in Fig. 3 above, for which the driving is essentially adiabatic and the oscillations are related to the amplitude rather than the frequency of the driving.

The same system has been studied in [9] as a prototypical example of a strongly damped system undergoing a transition from an energetically lower well to the higher well induced by external driving. The calculations in [9] were carried out within the noninteracting-blip approximation and the interacting-blip chain approximation. The validity of these approximation methods are confirmed by the present QMC simulations.

B. Nondiagonal driving force

Up to this point, we have discussed systems with an external force coupled diagonally to the two-state system. We now turn our attention to the influence of an external force that periodically modifies the intersite coupling element. In the case of a sinusoidal force the amplitude of the Δ_a must be smaller than the permanent coupling Δ_0 in order to avoid unphysical negative interstate coupling elements $\Delta(t)$.

1. Model I

In Fig. 5 the dashed line shows $\langle\sigma_z\rangle_t$ for model Ia with an oscillating interstate coupling element ($\nu_\Delta=\Delta_0$ and $\Delta_a=0.9\Delta_0$). Compared to the undriven case, the dynamics is modified in two ways. The transfer is slowed down considerably. The periodicity of the intertstate coupling element manifests itself in an enhancement or suppression of the transition rate. The effect is more significant the faster the transition is. In contrast to diagonal driving, the onset of the effect is instantaneous.

Next we investigate model Ib, which has an inversed static bias. As we have seen from Fig. 3, diagonal driving accelerates the transfer. This does not seem to be the case for off-diagonal driving. Within a series of simulations in the physically meaningful regime $\Delta_a\leqslant\Delta_0$, no enhancement of the transition could be found. However, minor acceleration and deceleration of the transfer due to the time-dependent interstate coupling element can be observed as well. For a frequency $\nu_\Delta=\Delta_0$ and an amplitude $\Delta_a=0.9\Delta_0$ of the driving force, this effect is illustrated in Fig. 6.

2. Model III

To further eludicate the effects of off-diagonal driving, we have also studied an unbiased system with $\alpha=0.25$ and cutoff frequency $\omega_c=5\Delta_0$ at low temperature $k_BT=0.1\Delta_0$, denoted model III. The amplitude of the time-dependent interstate coupling element is $\Delta_a=0.9\Delta_0$. In Fig. 7 the solid line represents the dynamics of the undriven system. The

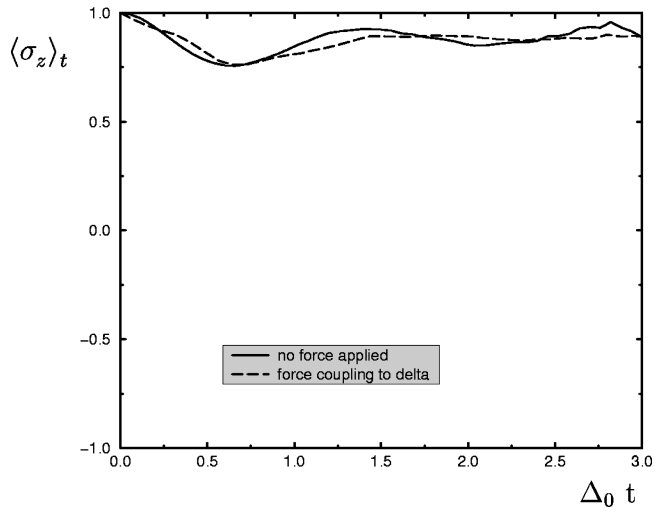

FIG. 6. $\langle\sigma_z\rangle_t$ for model Ib for different monochromatic driving coupled off diagonally. The solid curve corresponds to the undriven case. The dashed line has frequency $\nu_\Delta=\Delta_0$ and amplitude $\Delta_a=0.9\Delta_0$.

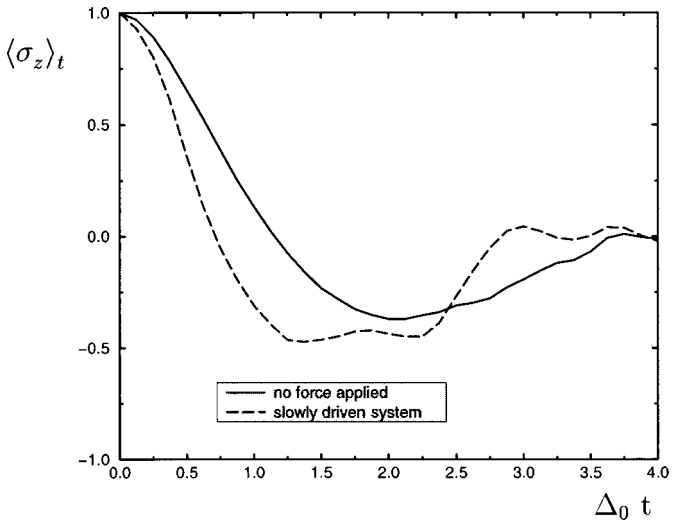

FIG. 7. Dynamics of a tunnel process of an unbiased system under a force coupling off diagonally. The electronic coupling is always $\Delta(t)=\Delta_0+0.9\sin(\nu_{\Delta_0}t)$. The other parameters are $k_BT=0.1\Delta_0$, $\alpha=0.25$, $\omega_c=5\Delta_0$, and $\nu_\Delta=0.5$. One can clearly observe the acceleration and deceleration effects.

dashed line shows the effects of a driving force with $\nu_\Delta=\Delta_0$. The same typical acceleration/deceleration effects, the slowing down and the instantaneous onset as we have observed in Figs. 6 and 4, remain. The impact of periodic driving decreases with increasing frequency. For an extremely high driving frequency of $\nu_\Delta=50\Delta_0$ the effects of the driving vanish almost completely. On the time resolution of our simulations, the average coupling element is uneffected by the rapidly oscillating time-dependent part of the interstate coupling element. Corresponding plots have therefore been omitted.

V. CONCLUSIONS AND OUTLOOK

The quantum Monte Carlo method for real- and complex-time path integration for the spin-boson model [7,26] has been extended to driven systems. The external field may couple diagonally as well as off diagonally to the two-state system. We studied periodic driving for both coupling mechanisms, but our method can be used to treat any other time-dependent driving force. The generalization to multistate tight-binding systems is also straightforward and permits a wide range of applications for the method. The possibility of controlling tunneling by external fields in two principally different ways has been demonstrated by numerical examples in the spin-boson model with Ohmic dissipation. By suitably adjusting the amplitude and frequency of the periodic driving force it is possible to quench as well as to activate tunneling. From a chemical perspective, the latter effect is interesting and relevant to the possibility of activating chemical reactions by external driving on the basis of microscopic processes. The methodology presented in this work can also simulate pump-probe experiments (see [50] and references therein) of electron transfer reactions in large biological molecules where the huge number of vibrational degrees of freedom can by modeled by a spectral density function that can be obtained from molecular dynamics simulations (see, for example, [10]). The ultrafast charge separation in bacterial photosynthesis is perhaps the most promising candidate for such simulations.

Another advantage of a numerically exact method is its application as a benchmark for various approximate methods. At least for short to intermediate times, the accuracy and the range of validity of approximate methods can be checked against QMC simulations.

In order to obtain complete information about the dynamics, the time evolution of the coherences [20] (i.e., off-diagonal elements of the reduced density matrix) must be known as well. Our ongoing work is focused on the modification of the algorithm to calculate the off-diagonal elements of the reduced density matrix.

As we have already mentioned, the QMC method does not invoke any approximation in the treatment of the driving force or the time-nonlocal interactions entering the influence functional. On the other hand, the method is computationally demanding. As the amount of the required computer memory is minor in comparison to the CPU time, it is perfectly suited for massive parallel computers with a distributed memory architecture.

ACKNOWLEDGMENTS

This work has been supported by the Deutsche Forschungsgemeinschaft (DFG) through the Sonderforschungsbereich 382. The authors would like to thank Reinhold Egger, Milena Grifoni, and Harald Weber-Gottschick for stimulating discussions. The calculations have been carried out on the Cray T3E and Paragon parallel computers of the *Rechenzentrum der Universität Stuttgart*. We gratefully acknoledge the support of Stefan Hüttemann concerning the efficient parallelization of the code in the context of the Sonderforschungsbereich 382 of the DFG. C.H.M. was also supported by the National Science Foundation (Grant No. CHE-9528121), the NSF Young Investigator Awards Program (Grant No. CHE-9257094), the Camille and Henry Dreyfus Foundation under the Camille Teacher-Scholar Award Program, and the Sloan Foundation.

[1] D. M. Eigler and E. K. Schweizer, Nature (London) **344**, 524 (1990).
[2] A. A. Louis and J. P. Sethna, Phys. Rev. Lett. **74**, 1363 (1995).
[3] S. Han, J. Lapointe, and J. E. Lukens, Phys. Rev. Lett. **66**, 810 (1991).
[4] R. A. Marcus and N. Sutin, Biochim. Biophys. Acta **811**, 265 (1985).
[5] D. Chandler, in *Liquids, Freezing, and the Glass Transition*, 1991 Les Houches Lectures, edited by D. Levesque *et al.* (Elsevier Science, Amsterdam, 1991).
[6] A. Benderskii, D. E. Makarov, and C. A. Wight, Adv. Chem. Phys. **88**, 1 (1994).
[7] R. Egger and C. H. Mak, Phys. Rev. B **50**, 15 210 (1994).
[8] R. Egger and C. H. Mak, J. Phys. Chem. **98**, 9903 (1994).
[9] M. Winterstetter and U. Weiss, Chem. Phys. **209**, 455 (1996).
[10] M. Marchi, J. N. Gehlen, and D. Chandler, J. Am. Chem. Soc. **115**, 4178 (1990).
[11] U. Weiss, *Quantum Dissipative Systems* (World Scientific, Singapore, 1993).
[12] R. P. Feynman, Rev. Mod. Phys. **20**, 367 (1948).
[13] R. P. Feynman and A. R. Hibbs, *Quantum Mechanics and Path Integrals* (McGraw-Hill, New York, 1965).
[14] L. S. Schulman, *Techniques and Applications of Path Integrals* (McGraw-Hill, New York, 1981).
[15] R. P. Feynman and F. L. Vernon, Ann. Phys. (N.Y.) **24**, 118 (1963).
[16] A. G. Redfield, Adv. Magn. Reson. **1**, 1 (1965).
[17] A. J. Leggett, S. Chakravarty, A. T. Dorsey, M. P. A. Fisher, A. Garg, and W. Zwerger, Rev. Mod. Phys. **59**, 1 (1987).
[18] M. Sassetti and U. Weiss, Phys. Rev. A **41**, 5383 (1990).
[19] R. Egger, C. H. Mak, and U. Weiss, Phys. Rev. E **50**, R655 (1994).
[20] M. Grifoni, M. Winterstetter, and U. Weiss, Phys. Rev. E **56**, 334 (1997).
[21] C. H. Mak and D. Chandler, Phys. Rev. A **44**, 2352 (1991).
[22] R. D. Coalson, D. G. Evans, and A. Nitzan, J. Chem. Phys. **101**, 436 (1994).
[23] N. Makri and D. E. Makarov, J. Chem. Phys. **102**, 4611 (1995).
[24] M. Winterstetter and W. Domcke, Chem. Phys. Lett. **236**, 445 (1995).
[25] J. T. Stockburger and C. H. Mak, Phys. Rev. Lett. **80**, 2657 (1998).
[26] C. H. Mak and R. Egger, Adv. Chem. Phys. **93**, 39 (1996).
[27] N. Makri, J. Math. Phys. **36**, 2430 (1995).
[28] E. Sim and N. Makri, Comput. Phys. Commun. **99**, 335 (1996).
[29] F. Grossmann, P. Jung, T. Dittrich, and P. Hänggi, Phys. Rev. Lett. **67**, 516 (1992).
[30] F. Grossman and P. Hänggi, Europhys. Lett. **18**, 571 (1992).
[31] J. M. Gomez Llorente, Phys. Rev. A **45**, R6958 (1992); Phys. Rev. E **49**, 3547(E) (1994).
[32] T. Dittrich, B. Oelschlägel, and P. Hänggi, Europhys. Lett. **22**, 5 (1993).
[33] B. Oelschlägel, T. Dittrich, and P. Hänggi, Acta Phys. Pol. B **24**, 845 (1993).
[34] Y. Dakhnovkii, Phys. Rev. B **49**, 4649 (1994).
[35] Y. Dakhnovkii, Ann. Phys. (N.Y.) **230**, 145 (1994).
[36] M. Grifoni, M. Sassetti, P. Hänggi, and U. Weiss, Phys. Rev. E **52**, 5863 (1995).
[37] M. Grifoni, Phys. Rev. E **54**, R3086 (1996).
[38] Yu. Daknovskii, J. Chem. Phys. **100**, 6492 (1994).
[39] Yu. Daknovskii and R. D. Coalson, J. Chem. Phys. **103**, 2908 (1995).
[40] A. Lucke, C. H. Mak, R. Egger, J. Ankerhold, J. Stockburger, and H. Grabert, J. Chem. Phys. **107**, 8397 (1997).
[41] I. A. Goychuk, E. G. Petrov, and V. May, Chem. Phys. Lett. **353**, 428 (1996).
[42] D. Makarov and N. Makri, J. Chem. Phys. **102**, 4611 (1995).
[43] D. G. Evans, R. D. Coalson, H. J. Kim, and Y. Dakhnovskii, Phys. Rev. Lett. **75**, 3649 (1995).
[44] M. Grifoni, L. Hartmann, and P. Hänggi, Chem. Phys. **217**, 167 (1997).
[45] M. Grifoni, M. Sassetti, P. Hänggi, and U. Weiss, Phys. Rev. E **52**, 3596 (1995).
[46] M. Grifoni, M. Sassetti, and U. Weiss, Phys. Rev. E **53**, R2033 (1996).
[47] M. Grifoni and P. Hänggi, Phys. Rev. Lett. **76**, 1611 (1996).
[48] D. G. Evans and R. D. Coalson, J. Chem. Phys. **104**, 2287 (1996).
[49] M. Grifoni and P. Hänggi, Phys. Rep. **304**, 230 (1998).
[50] W. Domcke and G. Stock, Adv. Chem. Phys. **100**, 1 (1997).
[51] M. F. Trotter, Proc. Am. Math. Soc. **10**, 545 (1959).